Remote Sensing of Environment 344 (2026) 115540

Contents lists available at ScienceDirect

Remote Sensing of Environment

journal homepage: www.elsevier.com/locate/rse

Basal area loss from fire using field-calibrated remote sensing refines western US fire severity measurements☆

Sara Winsemius [a,b,*], Yufang Jin [a], Hugh D. Safford [c], Michelle C. Agne [d], Robert A. Andrus [e], C. Alina Cansler [f], Anthony C. Caprio [g], W. Wallace Covington [h,i], Joseph E. Crouse [h], Calvin Farris [j], Peter Z. Fulé [k,i], Brian J. Harvey [l], Sharon M. Hood [m], David W. Huffman [h], Emma J. McClure [n], Alicia Reiner [o], John P. Roccaforte [h], Saba J. Saberi [c], Michael T. Stoddard [h], Laura Trader [p], Phillip J. van Mantgem [q], Micah C. Wright [q], Michael J. Koontz [r,s]

[a] Department of Land, Air and Water Resources, University of California, Davis, CA 95616, USA
[b] Currently at California Department of Forestry and Fire Protection, Fire and Resource Assessment Program, Sacramento, CA 95814, USA
[c] Department of Environmental Science, Policy and Management, University of California, Davis, CA 95616, USA
[d] USDA Forest Service, Pacific Northwest Research Station, ORISE Fellow, Olympia, WA 98512, USA
[e] School of the Environment, Washington State University, Pullman, WA 99163, USA
[f] Department of Forest Management, W.A. Franke College of Forestry and Conservation, University of Montana, Missoula, MT 59812, USA
[g] Division of Resources Management and Science, Sequoia and Kings Canyon National Parks, Three Rivers, CA 93271, USA
[h] Ecological Restoration Institute, Northern Arizona University, Flagstaff, AZ 86011, USA
[i] School of Forestry, Northern Arizona University, Flagstaff, AZ 86011, USA
[j] National Park Service, Interior Regions 8, 9, 10 and 12, Klamath Falls, OR 97603, USA
[k] Aix Marseille Univ, Avignon Univ, CNRS, IRD, IMBE, Marseille, France
[l] School of Environmental and Forest Sciences, College of the Environment, University of Washington, Box 352100, Seattle, WA 98195-2100, USA
[m] USDA Forest Service, Rocky Mountain Research Station, Missoula, MT 59808, USA
[n] National Park Service, Redwood National and State Parks, Orick, CA 95555, USA
[o] USDA Forest Service, Pisgah Forest, NC 28768, USA
[p] National Park Service, Pueblo and Four Winds Parks Fire Ecology, Los Alamos, NM 87544, USA
[q] U.S. Geological Survey, Western Ecological Research Center, Arcata, CA 95521, USA
[r] Vibrant Planet, PBC, Truckee, CA 96161, USA
[s] U.S. Geological Survey, Fort Collins Science Center, Fort Collins, CO 80526, USA

ARTICLE INFO

Keywords:
Basal area
Burn severity
Fire effects
Fire severity
Google earth engine
Random forest
Open-source workflow

ABSTRACT

The spatial patterns of fire effects and tree mortality have profound consequences for forest resilience. Cost-effective, medium-resolution, and spatiotemporally extensive fire severity measurements are essential for informing post-fire restoration and improving our understanding of wildfires—from forest stands to continents and from days to decades. Remote sensing advancements have improved burn severity mapping, but methods vary in interpretability, scalability, generalizability, and alignment with field measurements. One meaningful metric of fire effects on forests is proportion basal area loss, but existing methods are limited by a lack of region-specific field reference data and a scalable mapping framework. To address these issues, we compiled 3280 field reference plots from 123 fires in forests across the Western US to calculate the proportion of fire-induced basal area loss. We then used spatially cross-validated machine learning models with concurrent hyperparameter tuning to select a skillful, parsimonious model from a large candidate set of remotely-sensed, climatic, and topographic predictors. Spectral-only measures of severity over- or underestimated basal area loss in dry versus

☆ This article is part of a Special issue entitled: 'Medium and High Resolution Satellite' published in Remote Sensing of Environment.

* Corresponding author at: California Department of Forestry and Fire Protection, Fire and Resource Assessment Program, Sacramento, CA 95814, USA.
E-mail addresses: swinsemius@ucdavis.edu, sara.winsemius@fire.ca.gov (S. Winsemius), yujin@ucdavis.edu (Y. Jin), hdsafford@ucdavis.edu (H.D. Safford), Michelle.Agne@usda.gov (M.C. Agne), robert.andrus@wsu.edu (R.A. Andrus), alina.cansler@umontana.edu (C.A. Cansler), Tony_Caprio@nps.gov (A.C. Caprio), Wally.Covington@nau.edu (W.W. Covington), Joseph.Crouse@nau.edu (J.E. Crouse), Calvin_Farris@nps.gov (C. Farris), Pete.Fule@nau.edu (P.Z. Fulé), bjharvey@uw.edu (B.J. Harvey), sharon.hood@usda.gov (S.M. Hood), David.Huffman@nau.edu (D.W. Huffman), Emma_Mcclure@nps.gov (E.J. McClure), alicia.reiner@usda.gov (A. Reiner), John.Roccaforte@nau.edu (J.P. Roccaforte), sjsaberi@ucdavis.edu (S.J. Saberi), Michael.Stoddard@nau.edu (M.T. Stoddard), Laura_Trader@nps.gov (L. Trader), pvanmantgem@usgs.gov (P.J. van Mantgem), mcwright@usgs.gov (M.C. Wright), mikoontz@vibrantplanet.net (M.J. Koontz).

https://doi.org/10.1016/j.rse.2026.115540
Received 18 February 2026; Received in revised form 11 June 2026; Accepted 17 June 2026
Available online 12 July 2026

wet years and across aspects, demonstrating the value of incorporating climatic and topographic context. We also tested model performance on a separate holdout dataset in the Southwest US as a demonstration of reproducibility and transparency. We provide a Google Earth Engine tool for estimating proportional basal area loss for any fire perimeter in the Western US, enabling rapid map creation for land management and ecological modeling. All code, model parameters, and training data are released to support reproducibility, community adoption, regional refinement, and adaptation to new regions.

1. Introduction

Fire severity (sometimes called "burn severity") describes fire-induced changes to ecosystem components including soil and vegetation (Keeley, 2009; Morgan et al., 2014), and it is a crucial driver of ecosystem dynamics in fire-affected ecosystems, including disturbance-vegetation structure feedbacks, nutrient cycling, erosion, habitat creation and destruction, and successional pathways (Brodie et al., 2023; Cansler et al., 2022b; Keeley and Safford, 2016; Lutz et al., 2020; Turner, 2010). Due to the spatiotemporally heterogeneous nature of fire extent and severity, fire severity mapping depends on remote sensing linked to ground-level data to provide ecologically meaningful products and tools. The application of multispectral medium-resolution satellite imagery has been critically important for observing spatial and temporal patterns and trends in fire severity (Eidenshink et al., 2007; Radeloff et al., 2024).

By providing standardized measurements with spatiotemporally extensive sampling, remote sensing has transformed our understanding of fire effects. Satellite-derived spectral indices are used to measure fire severity, including delta normalized burn ratio (dNBR), relativized delta normalized burn ratio (RdNBR), and relativized burn ratio (RBR) (Key and Benson, 2006; Miller and Thode, 2007; Parks et al., 2014). These indices measure the change in reflectance after fire and are most commonly used with data from Landsat Thematic Mapper (TM), Enhanced Thematic Mapper Plus (ETM+), Operational Land Imager (OLI), or Sentinel-2 imagery. Spectral severity indices are used either directly or they are transformed into metrics based on correlations with field-based measures of fire severity such as the Composite Burn Index (CBI), a standardized post-fire protocol that combines estimates of percent change from five strata from soil to trees on a scale of 0–3 (Key and Benson, 2006; Miller et al., 2023, Miller et al., 2009; Saberi et al., 2022). Historically, these indices were computed using a single pre-fire and a single post-fire image, visually selected by an analyst to ensure the highest possible quality image (e.g., low cloud cover). Cloud computing platforms such as Google Earth Engine (GEE; Google LLC, Mountainview, CA) reduced personal computational requirements to calculate per-pixel averages of several images, which reduced the reliance on single images and intraannual phenological differences between pre- and post-fire imagery captured at different times of the year (Parks et al., 2018). Fire severity maps have been essential for understanding many ecological processes, including departure in severity and patchiness from historic conditions and post-fire vegetation recovery, and also for guiding postfire management response (Eidenshink et al., 2007; Steel et al., 2018; Stewart et al., 2021; Williams et al., 2023).

Ecological meaning of fire severity maps is inferred from a variety of current mapping methods, with varying interpretability. Key federal programs for severity mapping have been instrumental for integrating severity into research and management decisions. The Monitoring Trends in Burn Severity (MTBS) program produces dNBR and RdNBR, and then categorical maps of fire severity are produced subjectively by an analyst who determines the thresholds between classes for each fire (Eidenshink et al., 2007). The subjectivity of the MTBS fire severity assignments means that spatially or temporally disjunct fires should not be analyzed together (Kolden et al., 2015). Rapid Assessment of Vegetation Condition after Wildfire (RAVG) produces immediate and extended postfire RdNBR for large fires on National Forest System and Department of Interior lands only, and then applies threshold values to all forest lands to produce categorical layers for basal area (BA) loss, canopy cover loss, and CBI (Reiner et al., 2022). Until 2024, all Western US fires used thresholds determined by field measurements from only the Sierra Nevada (Miller et al., 2009), however extended assessments now separate California, Southwest and Northwest regions (Reiner et al., 2022; Saberi and Harvey, 2023). To provide more ecologically meaningful fire severity mapping compared to raw spectral measurements, Parks et al. (2019) introduced a framework to model CBI as a function of spectral measurements and other covariates in GEE. This approach formalized the ability to incorporate spatial and climatic context in the interpretation of spectral severity measurements (Parks et al., 2019).

While the use of CBI is common, it can be difficult to interpret as it is a composite index based on percent change of multiple strata (Key and Benson, 2006; Miller et al., 2023). However, CBI data has the benefit of having been previously assembled into geospatially-explicit formats suitable for training remote sensing-based models (e.g., Picotte et al., 2019, 2020; Parks et al., 2019), while fire severity metrics based on individual tree measurements exist disparately in datasets across regions, years, and research groups (Cansler et al., 2020). Yet, field-collected fire severity data based on individual tree measures, such as tree mortality, canopy cover change, or basal area loss, may provide even more utility in management contexts (Miller et al., 2009; Miller and Quayle, 2015). While the data require significant work to compile due to variation in protocol and data format (Cansler et al., 2020), they provide opportunities to map more ecologically relevant and interpretable metrics (Harvey et al., 2019; Whitman et al., 2018).

Land managers and researchers need maps of fire severity trained on local field data and informed by mechanistic covariates. One metric, basal area (BA) loss, measures the proportional change in the cross-sectional area of tree stems at breast height and is a common way to describe tree mortality and biomass loss due to fire. Fire severity has often been modeled using individual remotely sensed fire severity indices (Eidenshink et al., 2007; Miller and Thode, 2007; Parks et al., 2014), and more recently with additions of other spectral information and climatic and geographic variables that help in distinguishing how fire effects may differ across space (Furniss et al., 2020; McCarley et al., 2017; Parks et al., 2019; Viedma et al., 2020). Mechanistic variables such as climate and topography are more often used as predictors in the analysis of fire severity data than in their creation. However, biophysical conditions can change the relationship between spectral imagery and BA loss measures (Harvey et al., 2019) and climatic means can be useful in distinguishing fire effects across different regions (Parks et al., 2019). Climate conditions prior to or after the fire can be important drivers of fire severity (Barker et al., 2022; Cansler et al., 2024; Furniss et al., 2020; van Mantgem et al., 2013). They may also be important for adjusting the interpretation of a spectral imagery signal due to the mixed signal of tree mortality and understory response, though to our knowledge this has not been studied before.

Our main goal was to create an accessible, reproducible, and rigorous tool to calculate vegetation-based fire severity (hereafter "fire severity") with an easily interpreted metric (BA loss) across time and space that is immediately operational in the Western US and is extensible to other fire-prone forest ecosystems globally. Our specific objectives included to 1) assemble a shareable, geolocated BA loss field dataset, 2) determine the best model for estimating BA loss across the Western US using a robust machine learning approach, 3) illuminate the ecological implications of important variable interactions in the best model, 4) assess the model performance for a general Western model and for ecoregion-specific models, and 5) provide an open-access tool for mapping fire severity. We trained the model on BA loss data from across the region and assembled ecologically meaningful spectral, climatic, and topographic covariates. We integrated spatially blocked cross-validation, automated hyperparameter tuning with feature selection, and ecoregion-specific modeling to optimize predictive skill while minimizing over-fitting, advancing best practices for large-area accuracy assessment. All code, model parameters, and training data are available in an analysis-ready format to foster reproducibility and community adoption. Rapid map delivery and open licensing position the GEE tool for immediate use in land management planning, National Environmental Policy Act (42 U.S.C. § 4321 et seq.) analyses, and long-term monitoring. The resulting maps directly support post-fire treatment prioritization, carbon accounting, and ecological modeling.

2. Methods

We developed machine learning models to link the field measurements with remote sensing observations from Landsat. Due to the ecological, climatic, and topographic diversity of the study area, additional environmental covariates, including several climatic and topographic variables, were also explored for inclusion in the model for a more robust performance (Table S1). All potential predictors were calculated and extracted using the GEE cloud computing platform (Gorelick et al., 2017).

2.1. Field reference data

BA describes the cross-sectional area of tree stems at breast height. We acquired BA loss data from multiple sources, using published datasets (Cansler et al., 2020; Cansler et al., 2022a; McIver et al., 2016; Saberi et al., 2022) and agency datasets from the National Park Service (Supplements 3, 4). We included wildfire and prescribed fire datasets collected 0–3 years post-fire, and a subset contained pre-fire field measurements. Plot data needed to have a fixed plot size, include measurements of diameter at breast height (DBH) with tree status (live/dead), and have plot locations published or shared from collaborators. We drew heavily on the Fire and Tree Mortality (FTM) database (Cansler et al., 2020; Cansler et al., 2022a), which aggregated and standardized field observations, and obtained the associated plot locations from individuals and projects (Supplement 3).

We focused on the Western mountain forested ecoregions of the US (Fig. 1). The majority of plots were located in coniferous forests, though some represent deciduous or mixed forest. Our final dataset consisted of 3280 plots across 123 fires that burned from 1993 to 2017. Of these plots, 97 were sampled once after a prescribed fire and once again after a subsequent wildfire so are represented as 194 plots in our final dataset. Supplements 2 and 3 list the fires used in our study and the sources from which we obtained the data. Because we relied on many distinct field projects, we included plots with varying plot size and minimum DBH and with variable plot location accuracy. For data that included measurements from multiple years, we prioritized 1 year post-fire measures because it was the most common assessment and to correspond with spectral imagery; when those were not available, we used year-of-fire or 2 years post-fire, and then 3 years post-fire as needed. For the NPS data with pre-fire measures available, BA loss was calculated as $(BA_{live\_prefire} - BA_{live\_postfire}) / (BA_{live\_prefire})$, and when we only had post-fire measurements, as $(BA_{dead}) / (BA_{total})$. In the latter situation, we assumed that no trees were totally consumed and that boles remained because the boles that contributed to significant basal area likely remained except in extreme high severity patches (Lutz et al., 2020), and those plots would still have 100% BA loss without smaller trees in the data. Additionally, plots with only post-fire measurements excluded trees that field crews identified as dead before the fire (Cansler et al., 2020). We do not examine the effect of prior bark beetle attack on model accuracy, however it could be an important factor along with pre-fire stand structure.

2.2. Remote sensing data

The main inputs for our models came from multi-spectral imagery from Landsat satellites. The Landsat series, with the TM from 1984 to 2013 (Landsat 5), ETM+ sensor from 1999 to 2024 (Landsat 7), and OLI sensor from 2021 (Landsat 8 and 9), provides multispectral 30 m images covering the visible and infrared part of the spectrum every 16 days from each sensor (Earth Resources Observation and Science (EROS) Center, 2020a, 2020b, 2020c). We used Level 2, Collection 2 atmospherically corrected surface reflectance for six bands, available from GEE.

Image season was determined based on average green-up and

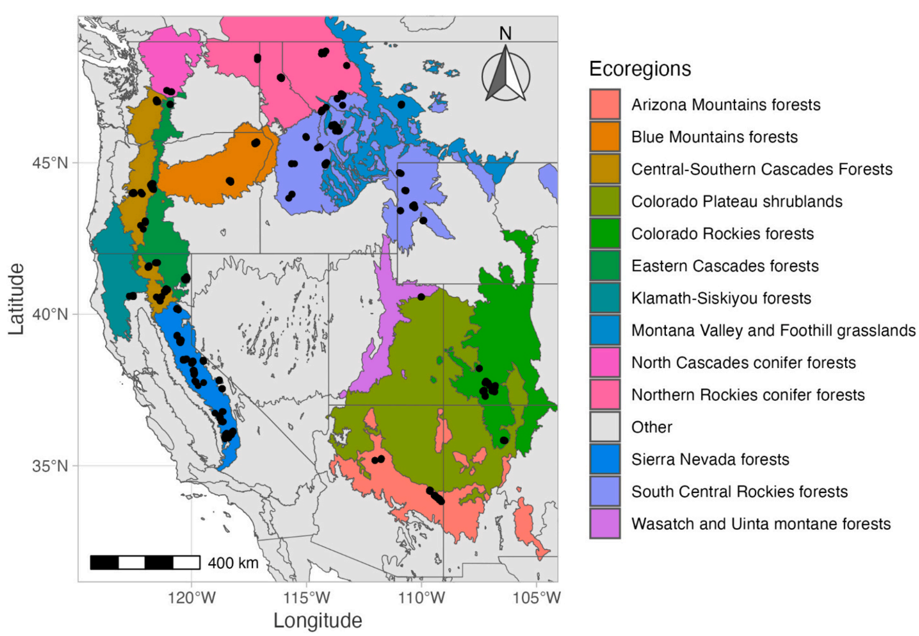

Fig. 1. Map of study area with 3280 plot locations (black dots) and ecoregions from RESOLVE (Dinerstein et al., 2017).

senescence dates for each of the RESOLVE ecoregions (Fig. 1) (Dinerstein et al., 2017). Using the Visible Infrared Imaging Radiometer Suite-derived annual Land Surface Phenology data (Zhang, 2024), we calculated the temporal per-pixel mean of the mid-greenup phase over 10 years (2013−2022) as the image season start and the per-pixel mean of the mid-senescence phase as the image season end, and used zonal statistics for each RESOLVE ecoregion to calculate the spatial mean image season start and end dates (Table S2).

For each Landsat image within the image season we masked cloud, cloud shadow, snow, ice, and water pixels. Each spectral band and index layer was then resampled using bilinear interpolation for smoother spatial transitions and improved representational accuracy (Cansler and McKenzie, 2012; Koontz et al., 2020) We then applied a mean compositing approach for each pre-fire and post-fire year, stacking and averaging all non-masked pixels within the image season for each spectral variable (Parks et al., 2018). In case of no clear images in the year pre- or post-fire, we used imagery from 2 years pre- and post-fire instead. Each differenced reflectance for a particular spectral band, index, and band ratio has been examined in the fire severity literature and is related to tree mortality—see Table S1 for citations. We extracted 6 individual band differences (red, green, blue, near infrared [NIR], and shortwave infrared 1 [SWIR1] and 2 [SWIR2]); snapshot indices for pre-fire enhanced vegetation index (EVI) and post-fire NBR and mid-infrared bi-spectral index (MIRBI); snapshot and differenced band ratios for SWIR1/NIR, SWIR2/NIR, and SWIR2/SWIR1; and 8 differenced indices with dNBR, RBR, RdNBR, delta normalized differenced vegetation index (dNDVI), dEVI, dMIRBI, delta near-infrared reflectance of vegetation (dNIRv), and delta normalized differenced moisture index (dNDMI) (Table S1).

2.3. Other explanatory variables: Climatic and topographic data

We examined climatic variables that show long-term climatic gradients, which drive vegetation distribution, as well as year of fire and 1 year post-fire weather variables that could influence fire intensity, tree responses after fire, and spectral reflectance (Table S1). Climate data were sourced from TerraClimate, which is a monthly climate and climatic water balance dataset available worldwide at 4 km resolution (Abatzoglou et al., 2018). We extracted data at plot centers. As climatic gradients control the distribution of vegetation, we calculated the 30-year average growing season climatic water deficit (CWD), vapor pressure deficit (VPD), actual evapotranspiration (AET), and total water-year precipitation. CWD, VPD, and AET were calculated for the warm season (May to September) (Alizadeh et al., 2021), while precipitation was calculated for the water year, October 1 to September 31. For year of fire and year post-fire, we calculated the same variables. We then calculated z-scores for the annual climate variables as, for example, $(CWD_0 - CWD_{mean}) / CWD_{stddev}$, where mean and standard deviation are calculated across 30 years from 1981 to 2010.

We calculated topographic variables using the USGS 10 m digital elevation model (DEM) (U.S. Geological Survey, 2025). Using plot centers and a 30 m radius, we obtained zonal statistics for elevation, and calculated slope, aspect in radians (with cos(aspect) and sin(aspect) to obtain “northness” and “eastness”, respectively), mean topographic position index (TPI), and heat load index (HLI) (Theobald et al., 2015). Mean TPI was derived from the 30 m Shuttle Radar Topography Mission DEM by averaging TPI across 270 m, 810 m, and 2430 m neighborhoods, and ranges from negative values (valleys) to positive values (ridges) (Theobald et al., 2015).

2.4. Random forest model

Machine learning methods including random forests have become common in ecological applications due to their flexibility and ability to reduce bias and overfitting (Breiman, 2001; Hudak et al., 2020; Powell et al., 2010). We used random forest models, simultaneously tuning model hyperparameters and selecting variables to reduce redundancy among the highly collinear predictors in the full dataset.

Initial model development was done in R using all explanatory variables (Table 1) to predict basal area loss as defined in Section 2.1 (R Core Team, 2024). Because the climatic predictor data are available at coarser spatial scales than the distance of plots within fires, multiple plots may share some identical predictor values, effectively reducing the number of independent observations. To mitigate the effects of spatial autocorrelation, we used a 10-fold spatial cross validation with k-means clustering using the spatialsample package (Brenning, 2012) ensured that the model evaluation was based on spatially independent subsets of withheld data by fitting a variogram to the cross-validated model residuals, determining the range to be 4.6 km, then calculating the pairwise minimum distance between blocks to be 159 km. We performed random forests using the ranger package (Wright and Ziegler, 2017) with the mlr3 learning structure (Lang et al., 2019). We simultaneously tuned the model's hyperparameters and reduced the feature set to only “important” features to yield a parsimonious, skillful model.

A challenge with typical, marginal measures of feature importance is that they perform poorly when features are correlated (Strobl et al., 2008; Watson and Wright, 2021). To determine feature importance more reliably with a correlated feature set, we used conditional predictive impact (CPI) with the cpi package (Watson and Wright, 2021), which measures the difference in model skill using the actual observed values compared to values derived using knockoff statistics for each feature in turn (Candès et al., 2018). Knockoff statistics replace the observed values of features (i.e., covariates/predictors) with values that break the relationship between the feature and the target, but retain the autocorrelation structure between the feature and other features. Greater CPI implies that the feature contributes more to model skill, conditional on the correlation structure of the features. The CPI approach allows for more robust measurement of feature importance for correlated features. Model skill was measured using log loss, and features were determined to be important if the lower bound of the CPI confidence interval derived using a Student's t distribution was greater than 0. We iterated across a grid of 720 combinations of hyperparameters: 3–12 variables per split (which limited the potential number of resulting variables in the model to 12); bag fraction values of 0.4, 0.5, 0.632, 0.7, 0.8 and 0.9; and minimum leaf population values of 1, 5, 10, 25, 50, 60, 70, 80, 90, 100, 125, and 150.

We then reran a random forest for each hyperparameter set using the important features and the same spatial folds, and calculated overall model R^2, RMSE, and MAE across all withheld testing data as well as the average model R^2, RMSE, and MAE across the ten spatial folds. We removed models from consideration when they had variables with Pearson correlation of 0.85 or greater. The final model and hyperparameter set was chosen by calculating the Pareto frontier for the overall R^2 and the number of variables in the model (Williams et al., 2019). We chose the final model by weighing four priorities: maximizing overall R^2, maximizing the mean R^2 across spatial folds, minimizing correlation between variables, and minimizing the number of variables in the model. This enabled us to maintain a high, though not the highest, R^2 while achieving a parsimonious model with fewer correlated predictors. This final model's hyperparameters and variables were then used in the GEE prediction. We visualized the effect of important features in the final model with the shape and magnitude of accumulated local effects (ALE) plots. ALE plots are an interpretation technique similar to partial dependence plots for black-box models such as random forests, but which provide more reliable information on feature contributions to model predictions when features are correlated (Apley and Zhu, 2020). Plots were created using the ale package (Okoli, 2023, 2025).

We also used similar methods to find the best model for each ecoregion. We used 5-fold spatial cross-validation for ecoregions with fewer than 300 plots and 10-fold cross-validation for ecoregions with more than 300 plots, and applied the same CPI approach as the general model.

Table 1
Model skill for each ecoregion by the general model and the ecoregion-specific models. See Fig. 1 for ecoregion locations. The general model used the equation RdNBR + dNIR + northness + zPrecip1 with mtry 3, sample fraction 0.632, and min node size 50. A few fires that spanned the border of two ecoregions were combined for calculating R^2 in this table: the California interior chaparral and woodlands plot was relabeled Klamath-Siskiyou forests and 7 Great Basin shrub steppe plots were combined with Sierra Nevada forests. The ecoregion-specific models specify the hyperparameters and important variables. Bolded R^2 values are those where the ecoregion model outperformed the general model for that region's testing data. See Table S1 for variable definitions.

Ecoregion	Number of plots	General model R^2	Ecoregional model mtry	Sample fraction	Min node size	Formula	R^2
Arizona Mountains forests	470	0.199	4	0.7	1	dNDMI + dSWIR1 + SWIR2SWIR1 + $Precip_{mean}$ + $zCWD_1$ + $zVPD_0$	**0.526**
Blue Mountains forests	217	0.604	3	0.4	70	dBlue + dRed + MIRBIpost + $SWIR1NIR_{pre}$ + $zAET_0$ + $zCWD_0$	−0.012
Central-Southern Cascades Forests	379	0.686	3	0.5	70	dSWIR1NIR + CWD_{mean} + $zPrecip_0$	**0.728**
Colorado Plateau shrublands	19	0.447	NA	NA	NA	NA	NA
Colorado Rockies forests	358	0.468	4	0.632	25	dNIRv + dSWIR2NIR + $zCWD_0$ + $zVPD_0$	**0.546**
Eastern Cascades forests	202	0.459	3	0.9	1	dSWIR1 + $MIRBI_{post}$ + HLI + slope	**0.652**
Klamath-Siskiyou forests	27	−3.162	3	0.8	5	dSWIR1 + dMIRBI + TPI	**0.204**
Montana Valley and Foothill grasslands	96	−0.318	4	0.5	25	dNIRv + dSWIR2 + VPD_{mean} + $zAET_0$	**0.360**
North Cascades conifer forests	12	0.895	4	0.5	1	dGreen + $SWIR1NIR_{pre}$ + $zCWD_0$ + $zPrecip_0$	−0.116
Northern Rockies conifer forests	241	0.119	3	0.7	90	dRed + dNIR + northness + $zAET_1$ + $zCWD_0$ + $zPrecip_0$	**0.412**
Sierra Nevada forests	811	0.428	4	0.4	90	dNDVI + $SWIR1NIR_{post}$ + northness + $zPrecip_1$	**0.470**
South Central Rockies forests	403	0.658	3	0.5	5	dNBR + TPI + VPD_{mean}	**0.660**
Wasatch and Uinta montane forests	45	−0.174	NA	NA	NA	NA	NA

We used the same Pareto frontier model selection procedure as for the general model.

Fire severity estimations are often grouped into categorical bins from low to high severity for model performance assessment (Brodie et al., 2023; Reiner et al., 2022; Stewart et al., 2021; Welch et al., 2016). After the continuous predictions we grouped the observed and predicted values into five classes and assessed the categorical model performance: < 25, ≥ 25 and < 50, ≥ 50 and < 75, ≥ 75 and < 90, and $\geq 90\%$ BA loss. This allowed us to assess model performance at different levels of severity.

The GEE code for producing all variables in Table 1 is available, along with the R code to run the variable selection procedure. Users with additional field training data can add it to the model training dataset, and, if desired, rerun the variable selection and tuning procedure to modify the GEE model. Note that the model selection process takes considerable computing time (~30 h parallelized across 10 cores with an Intel Core i7-8700K 3.70-GHz CPU processor; Intel Corporation, Santa Clara, CA). Code is available at https://github.com/swinsem/severity and data are available at https://osf.io/wmy2f/. All plot data are posted with BA loss, GEE covariates, and locations, except for National Park Service data which are provided without locations.

2.5. Model implementation

The process of extracting chosen explanatory variables, determination of image season, model execution, and prediction of mapped proportion BA mortality was run entirely in GEE using the variables and hyperparameters chosen in R. We provide code and training data to map basal area mortality across 5 sample fires. A user can run the code for any fire since 1985 in the Western US by uploading a fire perimeter with FireYear and FireID attributes. Because BA loss applies only to forested areas, users should only use the end product to evaluate fire severity in forests.

To demonstrate the model's ability to be tested with a new field dataset, we assessed the model's performance for a publicly available dataset of 338 plots measured one year after fire in Arizona and New Mexico from the Southwest US (Reiner et al., 2022); we present it as a vignette so that others may adapt it to datasets in other regions globally. All R code and a link to the open GEE script can be found at https://github.com/swinsem/severity.

3. Results

The random forest model predicting proportion basal area loss performed well across the Western United States (Table 1), with overall cross-validated model skill of $R^2 = 0.57$, RMSE = 0.27, and MAE = 0.20, and across spatial folds mean $R^2 = 0.39$ and median $R^2 = 0.51$. The model selection procedure yielded a model with four variables, describing basal area loss as a function of RdNBR, dNIR, northness, and $zPrecip_1$ (Table S1, bold), with mtry = 3, sample fraction = 0.632, and minimum node size = 50. We selected the model on the Pareto frontier based on greater parsimony, lower correlation between covariates, higher overall R^2, and higher R^2 across spatial folds (Fig. S1). Model performance varied greatly across ecoregions, with R^2 ranging from −3.16 to 0.895 (Table 1, Fig. 2). Note that the ecoregions and spatial folds are not exactly matched.

Most ecoregions had better performance with ecoregion-specific models than the general model (Table 1). Arizona Mountains forests had a notable improvement, with a jump in R^2 from 0.199 to 0.526. The Colorado Plateau shrublands and Wasatch and Uinta montane forests ecoregional models did not run successfully, possibly due to small spatial fold sizes.

We started model selection with 41 variables and the final model chosen had four: RdNBR, dNIR, z-score of precipitation from October of the fire year through September of the year after the fire ($zPrecip_1$), and northness (cos[aspect]). First order effects are shown with accumulated local effects (ALE) plots, which are better reflections of these effects than partial dependence plots when features are correlated (Fig. 3). The most important variable was RdNBR, which had a steep positive curve (99% of plots were below 1300); higher severity plots had higher RdNBR values. The $zPrecip_1$ curve was jagged, but in general BA loss increased for positive z-scores (wetter than average) and decreased for negative z-scores (drier than average years). The dNIR signal was near 0 for most of the range, perhaps due to redundancy with RdNBR, with a positive effect on BA loss for the roughly 10% of data with negative dNIR values. BA loss increased at northness values near 1 (due north) and decreased at

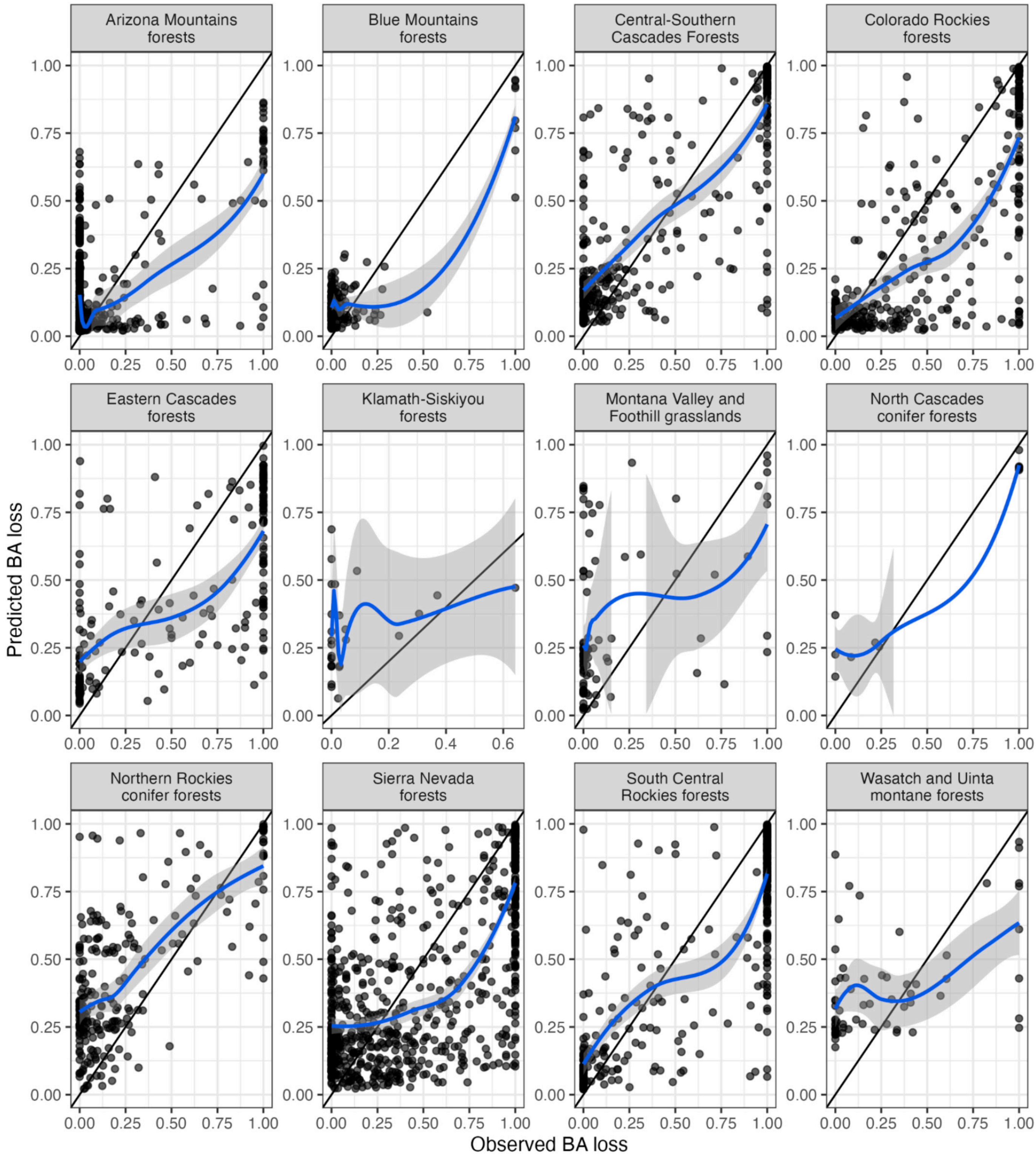

Fig. 2. Predictions and observations for proportion BA loss from the general model, displayed by ecoregion. The straight black line is the 1:1 line, while the blue line is the loess smoothed regression. The grey bars show the 95% confidence interval for the regression line and are missing if the range spans above 1 or below 0. Colorado Plateau shrublands are included with Wasatch and Uinta montane forests due to plot proximity to the boundary. See Table 1 for sample sizes of each ecoregion. (For interpretation of the references to colour in this figure legend, the reader is referred to the web version of this article.)

−1 (due south). We also visualized interactive effects of z-score precipitation and northness on the spectral signature of RdNBR in the raw data (Fig. 4). Interactions in the model are visualized in second-order effects ALE plots in Supplement 1 (Fig. S3).

We grouped the observed and predicted BA loss values into five classes: < 25, ≥ 25 and < 50, ≥ 50 and < 75, ≥ 75 and < 90, and ≥ 90% BA loss (Fig. S4). We did not use an unburned 0% loss class as seen in most other studies because our predictions had a minimum of 1% BA loss. When binned into these five severity categories, overall accuracy was 56% and Spearman's rank correlation coefficient was 0.71. The

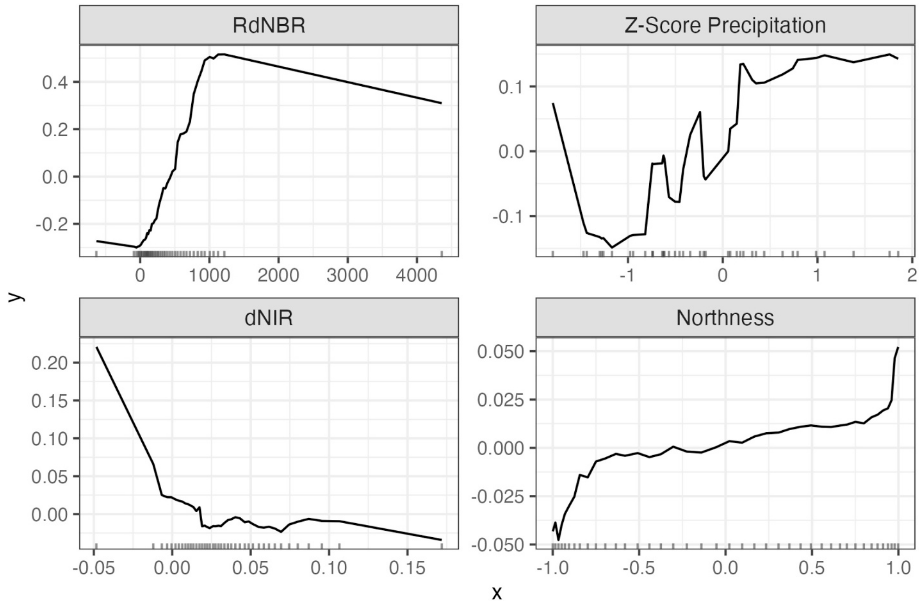

Fig. 3. Accumulated local effects (ALE) plots showing the first order effects of the four variables in the final model. The tick marks at the bottom of the graphs show the distribution of feature values for each variable. The y axis represents the effect of the variable on the output variable relative to the mean prediction, in the scale of the basal area (BA) loss output. For example, at high RdNBR values, the model predicts higher proportion BA loss.

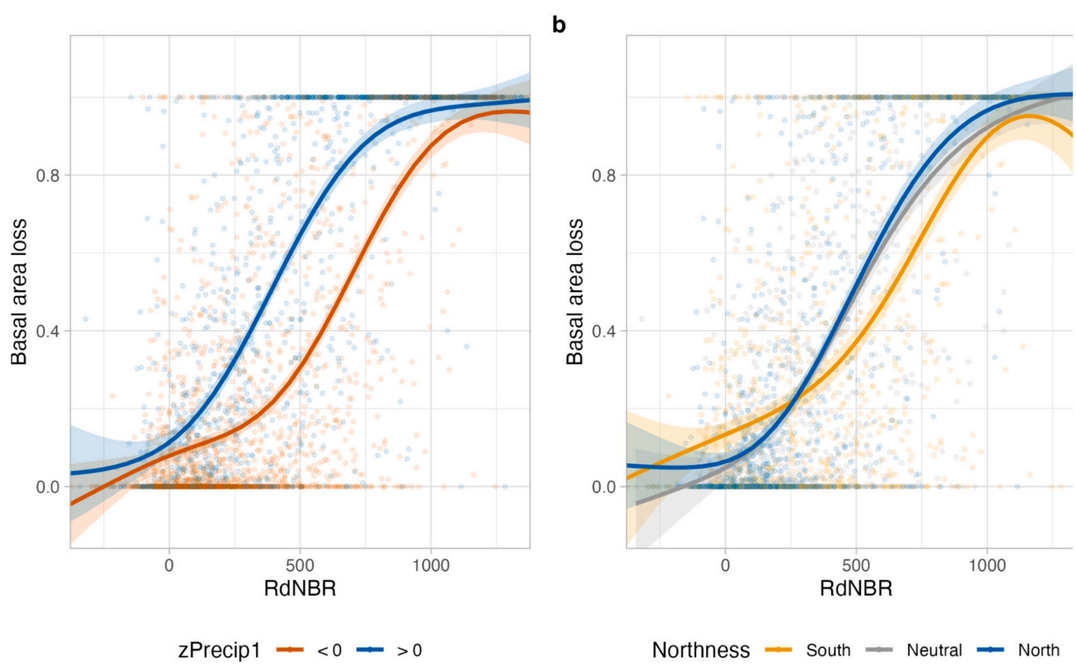

Fig. 4. Effects of northness and precipitation anomaly on the spectral signal of proportion basal area loss in RdNBR. The index values are more positive for higher severity burns. Smoothed lines show the GAM model and shaded regions indicate the 95% confidence interval for the lines. A. Effect of precipitation anomaly between the fire and the imagery year on how RdNBR predicts basal area (BA) loss ($zPrecip_1$). B. Effect of northness on the RdNBR relationship with BA loss, where northness is cos(aspect) with due north at 1, and neutral set as 0.33 to 0.66. At 50% BA loss, a plot that burned before a dry winter would look like it burned at higher severity than a plot that burned before a wet winter, by imagery alone. Or, at the same moderate spectral measurement (RdNBR = 500), a modeled estimate of BA loss would likely underestimate actual BA loss with a wet post-fire year, and overestimate actual BA loss with a dry post-fire year.

lowest and highest severity classes had high precision (positive predictive value) (0.82 and 0.91 for $< 25\%$ and $> 90\%$ BA loss, respectively) and high balanced accuracy (0.78 and 0.69, respectively) but the three intermediate classes had low precision (0.05 to 0.17) and balanced accuracy (0.54 to 0.56). Sensitivity, the true positive rate, was highest for low severity (0.75) with other classes ranging from 0.19 to 0.39. Specificity, the true negative rate, was relatively high across all classes, ranging from 0.81 to 0.99.

The model implementation in GEE displays or exports proportional BA loss at 30 m scale for any uploaded fire perimeter since 1985 (Fig. 5). We also tested the model with a new dataset of BA loss from the Southwest US as a proof of concept for assessing model skill in either a local area within our study area or a different region outside the Western US. R^2 was 0.48 for the fully heldout Southwest dataset, which closely aligned with our expectation based on the R^2 measured for the Arizona Mountains forests, Colorado Plateau shrublands, and Colorado Rockies

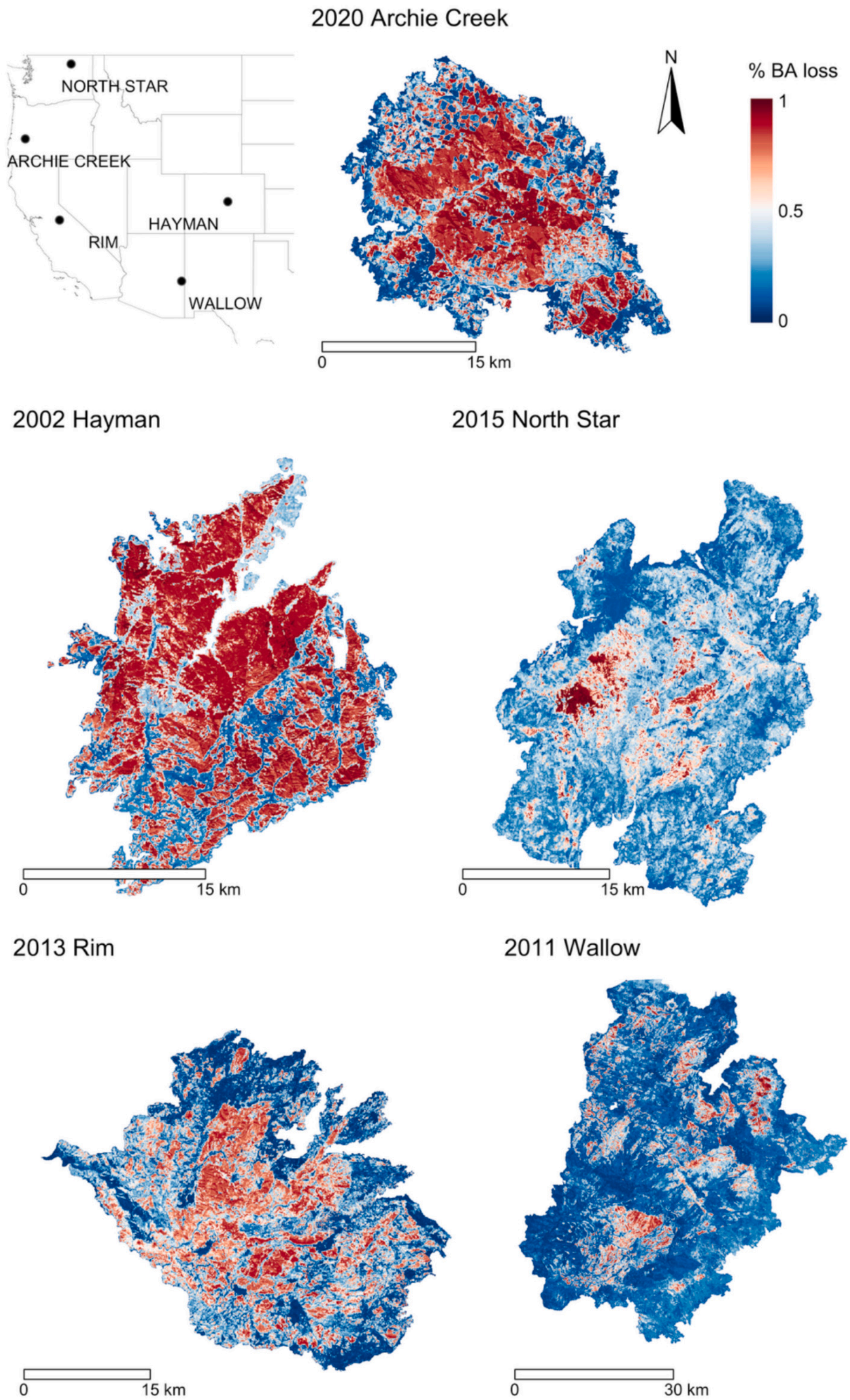

Fig. 5. Examples of predicted proportion of basal area (BA) loss for five selected fires. Note that these maps are shown for the full fire perimeters but BA loss is only valid for forested areas.

forests where the plots were distributed.

4. Discussion

4.1. General model skill and spatial variability

By assessing model skill across hyperparameter sets within a 10-fold spatial cross-validation, we used a rigorous model selection procedure that allowed us to balance the priority of overall model skill with spatially weighted skill. Our final model performed well across all plots, with variable performance across ecoregions. An ecoregion's performance in the general model was not highly correlated with the number of plots in the region. For example, we observed the highest R^2 in North Cascades conifer forests (0.895), which had only 12 plots, while the Sierra Nevada forests ecoregion, which had the most plots (811), had an R^2 of 0.428 (Table 1). Our field data also did not evenly represent the full spread of proportional BA loss in every ecoregion. In some regions, such as Utah's Wasatch and Uinta montane forests, model skill may improve with additional training plot data across the full range of proportional BA loss. Regional variation in model skill likely also reflects underlying ecological gradients in pre-fire stand structure and biomass density that our spectral predictors only partially capture, along with differences in seasonality between prescribed fires and wildfires.

We observed immense variation in performance between models with different hyperparameter sets, which demonstrates the importance of doing variable selection concurrently with hyperparameter tuning (Fig. S1). Overall mean R^2 varied from −0.33 to 0.59, while mean R^2 across spatial folds varied from −1.0 to 0.43. While many studies do not perform variable selection in concert with hyperparameter tuning—either because random forest is thought to work well enough with defaults or because it is computationally expensive (Fernandez-Delgado et al., 2014; Probst et al., 2019b, Probst et al., 2019a)—we believe it was an important step to find the best (i.e., skillful and parsimonious) model and that our cross-validation procedure prevented overfitting. The CPI process alone did not always result in models with uncorrelated variables, so we additionally filtered out models with covariates that had a Pearson correlation of 0.85 or higher. Our R^2 is lower than the Parks et al. (2018) CBI R^2 of 0.72, and there are certain regions where CBI prediction could be more reliable. However, some reduction in R^2 could be due to different cross-validation methods: they used a 5-fold cross-validation with a random 20% of fires held out for testing, while we used a 10-fold spatial cross-validation (or 5-fold for ecoregions with fewer than 300 plots) that withheld spatially grouped sets of plots.

Both the continuous and categorical BA loss revealed a similar pattern as is seen in other studies, with much better performance for the lowest and highest severity classes than the moderate severity (Miller et al., 2012; Miller and Safford, 2008; Miller and Thode, 2007). In the continuous results, very low and high BA loss anchor the predictions, with a wide range of estimates at moderate severity (Fig. 2). Some of this is expected because the spectral signal for low and high severity is more consistent and plots are more often contained within a larger patch size; moderate severity plots may be on the border of low and high severity patches or contain fine-scale patches of low and high severity (Miller and Thode, 2007). Additionally, we had a skewed number of plots within each bin, and particularly low numbers of plots at intermediate severity: 1781, 331, 186, 86, and 896 in each class from low to high. The high number of low severity plots is likely because we included prescribed fire plots along with wildfire plots.

4.2. Ecoregional models

Our primary goal was to create a model for consistent comparison of BA loss across the Western US, however we also tested ecoregion-specific models and provide the functions, hyperparameters, and model skill so that they may be applied as desired by a user. In most ecoregions R^2 improved with ecoregional models, with the biggest improvement in the Arizona Mountains. Some models had lower R^2 with the ecoregional models, however, perhaps due to the number and arrangement of spatial folds. Where training data are limited or in ecoregions that underperformed the general model, the general model remains a good choice for broad-area consistency.

Improved performance with local models would be expected due to the wide variety of pre-fire stand structures and disturbance regimes across the Western US. The diversity of variables in the ecoregional models suggests that the drivers of the spectral severity signal relative to BA loss are region-specific. For example, topographic variables dominated in the Eastern Cascades, while climate variables were central in the Arizona Mountains and South Central Rockies (Table 1). This reinforces the value of ecoregion-specific modeling where sufficient training data exist, while also highlighting the challenge of developing a single generalizable model across such ecologically diverse terrain.

4.3. Effects of climate and topography

The interpretation of the spectral signal of severity measured as basal area loss differs depending on climate and topography. We found that basal area loss would be underestimated on north slopes or when a wet winter follows a fire if the spectral index were used alone (Fig. 4). Conversely, basal area loss would be overestimated on south slopes or when a dry winter follows a fire if the spectral index were used alone. $zPrecip_1$, the z-score of precipitation in the water year of the imagery (October 1 of the fire year through September 30 of the year post-fire) was an important variable in all the formulas on the Pareto frontier for the general model. The first-order effect showed that higher precipitation is generally associated with higher BA loss (Fig. 3), which is similarly borne out in the raw data (Fig. 4), but we caution interpretation due to the high variability. As shown in the second-order ALE plots, post-fire precipitation anomaly interacts with RdNBR to increase severity predicted at moderate to high RdNBR during wet years and at low RdNBR in dry years, while reducing severity at high RdNBR in dry years and at low RdNBR in wet years (Fig. S3). Similarly, the strongest second-order effect of northness is at the hottest slope due south, where northness lowers severity at moderate-high RdNBR and increases it at low RdNBR. This could indicate that at moderate to high RdNBR, dry post-fire water year and warmer slopes correct even more for over-predictions in the imagery (an enhancement of the first-order effect of precipitation and northness), while at low RdNBR the first-order effects may be weakened.

While we might expect post-fire precipitation to increase tree survival, the model and data show more BA loss in wet years; similarly, other research has found that while pre-fire drought can increase fire severity, post-fire drought was not strongly predictive (Cansler et al., 2024; van Mantgem et al., 2013). The contribution of post-fire precipitation to model skill likely reflects multiple mechanisms that vary by ecoregion. In systems with significant herbaceous understory, wet post-fire years may promote rapid understory recovery that alters the spectral severity signal relative to actual overstory mortality. A similar spectral response could also be seen in the spectral response of forest canopy, based on greenness or dryness of remaining vegetation. This pattern could be less apparent in more mesic systems like the Central-Southern Cascades, where the spectral relationship between RdNBR and BA loss did not vary by precipitation as shown in Fig. 4. In general, though, we expect that the inclusion of precipitation improved model skill due to its interaction with RdNBR and dNIR: without including precipitation in the model, severity would be underestimated by the imagery alone in a wet post-fire year and overestimated in a dry post-fire year (Fig. 4a, Fig. S3). While post-fire precipitation may not have a clear influence on tree mortality, it strongly affects surface reflectance, with more moisture in vegetation in wetter years and less in drier years. We observed a similar but weaker effect with northness, without which the same BA loss would be over-predicted on warmer, drier south-facing slopes and under-predicted on cooler, wetter north-facing slopes. The effects of these variables are clear when plotting BA loss against RdNBR while separating wet from dry years and northern from southern slopes (Fig. 4). Second-order effects, which show a similar effect but using the model prediction rather than the raw data, are shown in ALE plots in Supplement 1 (Fig. S3). This is the first time to our knowledge that these variables have been used in fire severity mapping, and these results indicate that post-fire precipitation could be a key part of interpreting post-fire imagery.

The role of climate means and anomalies in the general and ecoregional models suggest at least three distinct mechanisms. In the Sierra Nevada, where z-score post-fire precipitation was the sole climate predictor selected for the ecoregional model, in the Northern Rockies where post-fire AET was selected, and in the Arizona Mountains where post-fire CWD was selected, wetter post-fire growing conditions appear to promote understory regrowth that lowers the spectral severity signal relative to actual overstory mortality, consistent with rapid revegetation. In contrast, some ecoregional models contain long-term mean climate variables, which reflect background aridity and site productivity. For example, increasing mean CWD in the Central-Southern Cascades is positively correlated with increasing BA loss, indicating that fire severity is higher in hotter, drier areas. In the South Central Rockies, however, mean VPD has a negative association with BA loss, which could indicate higher severity in the more mesic, high-elevation sites with higher biomass. Some ecoregions included a weak effect of fire-year climate. For the Central-Southern Cascades and Northern Rockies, a possible explanation of the positive relationship between fire-year precipitation and BA loss could be increased fine fuel continuity. Surprisingly, some ecoregional models include a negative relationship between BA loss and fire-year summer CWD or VPD, which could reflect a limited number of fires per year within the ecoregion and thus may indicate overfitting.

4.4. Next steps: Additional data and expansion to other regions

In future research, model improvements may be gained by grouping similar ecoregions; for example, Arizona Mountains could be combined with the Sierra Nevada because they both have predominantly dry mixed-conifer forests. Models could be created for three larger subregions similar to the current work by RAVG, with Southwest and Northwest regions separate from California, Nevada, Utah, and Colorado (Reiner et al., 2022; Saberi and Harvey, 2023). Alternatively, with enough field data, more local models with narrow ranges of pre-fire stand structure and disturbance history (i.e., beetle outbreak or recent prior fires) could improve models further (Harvey et al., 2019; Saberi and Harvey, 2023). While some research indicates pre-fire bark beetle outbreaks don't change fire detection accuracy with time-series methods (Rodman et al., 2021), multiple disturbances could impact severity predictions. While these efforts are outside the scope of our study, they would be interesting paths of further research.

All of the code necessary to expand on this project has been made available in GitHub and GEE. With additional local data, a user could test model performance for a field dataset anywhere globally so long as they have location data and calculated proportion BA loss, and we share code for doing this assessment using a held out dataset of plots from the Southwestern US (Reiner et al., 2022). The addition of local data could also be added to the training data and used to improve the model skill, and this code is also available. Plot locations can be uploaded to GEE to extract the spectral, climatic, and topographic training data. These can then be used either to simply test model fit or can be added to the full training dataset and added back to the prediction script in GEE. Reparameterizing the model is an additional option using R, however the process takes considerable computational resources.

This framework would also work in other regions worldwide given sufficient training data and a few simple modifications. The GEE code uses Landsat, Terraclimate, and a US-specific 10 m DEM; the DEM could be modified to use a global dataset at 30 or 90 m resolution. The RESOLVE ecoregions used for determining image season are also available globally (Dinerstein et al., 2017), and our code for determining image seasons is included in the GEE repository. For the code to be applied in the southern hemisphere, the variables for northness and heat load index would need to be modified. This could be done by calculating “southness” rather than “northness” by reversing the sign to calculate -cos(aspect) and adjusting the aspect folding reference in heat load index to 315 degrees rather than 225 degrees; these modifications are noted in the script provided. Additionally, the image season calculation may need to be modified, since mean green-up in southern hemisphere RESOLVE ecoregions could more likely occur later in the calendar year than mean senescence. One possible approach would be to define the image season as the time period between the mean green-up from two years prior to the fire year until the mean senescence from one year prior to the fire year. This would be in contrast to how we defined northern hemisphere image seasons as mean green-up to mean senescence, both one year prior to the fire year. While the model was trained and validated only using data from the Western US, the range of forest types included and mechanistic covariates may make this model more applicable to other regions globally than previous fire severity mapping methods. We suggest assessing and possibly retraining a new random forest model using our provided code when working outside the Western US.

5. Conclusions

We developed a model for BA loss after fire that includes a number of important advances. We trained on fires across space and time in the Western US, used mechanistic explanatory variables for climate and topography alongside spectral measurements, used a rigorous variable selection and hyperparameter tuning method to select the best model, and provided code so that the dataset and model can be applied to any fire perimeter and be updated with additional data. We found that spectral measurements alone may lead to important over- or underestimation depending on the precipitation between the fire and the image collection and on whether the plot is on a north- or south-facing slope. This indicates that the climatic and topographic circumstances are critical for correctly interpreting remotely sensed predictions of fire severity.

We created an operational GEE application for managers and researchers to map fire severity for any fire perimeter input from 1985 to one year before the analysis in the Western US. We provide additional code and data so that researchers can continue to improve on the model, especially in regions where we do not include as much training data. The application allows managers and researchers to map fire severity directly as BA loss using a generalized model across the Western US, enhancing our ability to interpret fire effects over space and time. We suggest assessing and possibly retraining the model before applying it in a new region, and provide code to facilitate the method's expansion into new areas.

CRediT authorship contribution statement

Sara Winsemius: Writing – review & editing, Writing – original draft, Visualization, Validation, Methodology, Formal analysis, Data curation, Conceptualization. **Yufang Jin:** Writing – review & editing, Funding acquisition. **Hugh D. Safford:** Writing – review & editing, Funding acquisition. **Michelle C. Agne:** Data curation. **Robert A. Andrus:** Writing – review & editing, Data curation. **C. Alina Cansler:** Writing – review & editing, Data curation. **Anthony C. Caprio:** Writing – review & editing, Data curation. **W. Wallace Covington:** Data curation. **Joseph E. Crouse:** Data curation. **Calvin Farris:** Data curation. **Peter Z. Fulé:** Data curation. **Brian J. Harvey:** Writing – review & editing, Data curation. **Sharon M. Hood:** Writing – review & editing, Data curation. **David W. Huffman:** Data curation. **Emma J. McClure:** Data curation. **Alicia Reiner:** Writing – review & editing, Data curation. **John P. Roccaforte:** Writing – review & editing, Data curation. **Saba J. Saberi:** Writing – review & editing, Data curation. **Michael T. Stoddard:** Writing – review & editing, Data curation. **Laura Trader:** Data curation. **Phillip J. van Mantgem:** Writing – review & editing, Data curation. **Micah C. Wright:** Writing – review & editing, Data curation. **Michael J. Koontz:** Writing – review & editing, Methodology, Formal analysis, Conceptualization.

Declaration of competing interest

The authors declare that they have no known competing financial interests or personal relationships that could have appeared to influence the work reported in this paper.

Acknowledgements

We acknowledge funding from Vibrant Planet, PBC that supported this work. Comments from Van Kane and Kevin Buffington improved this manuscript. Thanks to Jay Miller for the contribution of data. Many thanks to all the individuals who collected field data that went into this project. This work was supported by the U.S. Geological Survey Land Management Research Program and the National Park Service. Any use of trade, firm, or product names is for descriptive purposes only and does not imply endorsement by the U.S. Government.

Appendix A. Supplementary data

Supplementary data to this article can be found online at https://doi.org/10.1016/j.rse.2026.115540.

Data availability

We provide all code and data to produce mapped BA loss predictions for sample fires. Interested users can easily map BA loss for any fire from 1985 through the most recent fire year with complete post-fire data (available after the following September 30) in the Western US by uploading the fire perimeter(s) in the Google Earth Engine tool, a link to which is provided at this repository: https://github.com/swinsem/severity. Further, all data and code are available so that users may make modifications, such as adding field data and retraining the model, at the GitHub repository and at https://osf.io/wmy2f/. Location data is provided for all plots except the NPS and NPS_BAND datasets, which have locations fuzzed within a 1 mile radius and some locations swapped.

References

Abatzoglou, J.T., Dobrowski, S.Z., Parks, S.A., Hegewisch, K.C., 2018. TerraClimate, a high-resolution global dataset of monthly climate and climatic water balance from 1958–2015. Sci. Data 5, 170191. https://doi.org/10.1038/sdata.2017.191.

Alizadeh, M.R., Abatzoglou, J.T., Luce, C.H., Adamowski, J.F., Farid, A., Sadegh, M., 2021. Warming enabled upslope advance in western US forest fires. Proc. Natl. Acad. Sci. 118, e2009717118. https://doi.org/10.1073/pnas.2009717118.

Apley, D.W., Zhu, J., 2020. Visualizing the effects of predictor variables in black box supervised learning models. J. R. Stat. Soc. Ser. B Stat Methodol. 82, 1059–1086.

Barker, J.S., Gray, A.N., Fried, J.S., 2022. The effects of crown scorch on post-fire delayed mortality are modified by drought exposure in California (USA). Fire 5, 21. https://doi.org/10.3390/fire5010021.

Breiman, L., 2001. Random forests. Eur. J. Math. 45, 5–32. https://doi.org/10.1017/CBO9781107415324.004.

Brenning, A., 2012. Spatial cross-validation and bootstrap for the assessment of prediction rules in remote sensing: The R package sperrorest. In: 2012 IEEE International Geoscience and Remote Sensing Symposium. Presented at the 2012 IEEE International Geoscience and Remote Sensing Symposium, pp. 5372–5375. https://doi.org/10.1109/IGARSS.2012.6352393.

Brodie, E.G., Stewart, J.A.E., Winsemius, S., Miller, J.E.D., Latimer, A.M., Safford, H.D., 2023. Wildfire facilitates upslope advance in a shade-intolerant but not a shade-tolerant conifer. Ecol. Appl. 33, e2888. https://doi.org/10.1002/eap.2888.

Candès, E., Fan, Y., Janson, L., Lv, J., 2018. Panning for gold: 'model-X' knockoffs for high dimensional controlled variable selection. J. R. Stat. Soc. Ser. B Stat Methodol. 80, 551–577. https://doi.org/10.1111/rssb.12265.

Cansler, C.A., McKenzie, D., 2012. How robust are burn severity indices when applied in a new region? Evaluation of alternate field-based and remote-sensing methods. Remote Sens. 4, 456–483. https://doi.org/10.3390/rs4020456.

Cansler, C.A., Hood, S.M., Varner, J.M., van Mantgem, P.J., Agne, M.C., Andrus, R.A., Ayres, M.P., Ayres, B.D., Bakker, J.D., Battaglia, M.A., Bentz, B.J., Breece, C.R., Brown, J.K., Cluck, D.R., Coleman, T.W., Corace, R.G., Covington, W.W., Cram, D.S., Cronan, J.B., Crouse, J.E., Das, A.J., Davis, R.S., Dickinson, D.M., Fitzgerald, S.A., Fulé, P.Z., Ganio, L.M., Grayson, L.M., Halpern, C.B., Hanula, J.L., Harvey, B.J., Kevin Hiers, J., Huffman, D.W., Keifer, M., Keyser, T.L., Kobziar, L.N., Kolb, T.E., Kolden, C.A., Kopper, K.E., Kreitler, J.R., Kreye, J.K., Latimer, A.M., Lerch, A.P., Lombardero, M.J., McDaniel, V.L., McHugh, C.W., McMillin, J.D., Moghaddas, J.J., O'Brien, J.J., Perrakis, D.D.B., Peterson, D.W., Prichard, S.J., Progar, R.A., Raffa, K. F., Reinhardt, E.D., Restaino, J.C., Roccaforte, J.P., Rogers, B.M., Ryan, K.C., Safford, H.D., Santoro, A.E., Shearman, T.M., Shumate, A.M., Sieg, C.H., Smith, S.L., Smith, R.J., Stephenson, N.L., Stuever, M., Stevens, J.T., Stoddard, M.T., Thies, W.G., Vaillant, N.M., Weiss, S.A., Westlind, D.J., Woolley, T.J., Wright, M.C., 2020. The Fire and Tree Mortality Database, for empirical modeling of individual tree mortality after fire. Sci. Data 7, 194. https://doi.org/10.1038/s41597-020-0522-7.

Cansler, C.A., Hood, S.M., Varner, J.M., van Mantgem, P.J., Agne, M.C., Andrus, R.A., Ayres, M.P., Ayres, B.D., Bakker, J.D., Battaglia, M.A., Bentz, B.J., Breece, C.R., Brown, J.K., Cluck, D.R., Coleman, T.W., Corace, R.G., Covington, W.W., Cram, D.S., Cronan, J.B., Crouse, J.E., Das, A.J., Davis, R.S., Dickinson, D.M., Fitzgerald, S.A., Fulé, P.Z., Ganio, L.M., Grayson, L.M., Halpern, C.B., Hanula, J.L., Harvey, B.J., Kevin Hiers, J., Huffman, D.W., Keifer, M., Keyser, T.L., Kobziar, L.N., Kolb, T.E., Kolden, C.A., Kopper, K.E., Kreitler, J.R., Kreye, J.K., Latimer, A.M., Lerch, A.P., Lombardero, M.J., McDaniel, V.L., McHugh, C.W., McMillin, J.D., Moghaddas, J.J., O'Brien, J.J., Perrakis, D.D.B., Peterson, D.W., Prichard, S.J., Progar, R.A., Raffa, K. F., Reinhardt, E.D., Restaino, J.C., Roccaforte, J.P., Rogers, B.M., Ryan, K.C., Safford, H.D., Santoro, A.E., Shearman, T.M., Shumate, A.M., Sieg, C.H., Smith, S.L., Smith, R.J., Stephenson, N.L., Stuever, M., Stevens, J.T., Stoddard, M.T., Thies, W.G., Vaillant, N.M., Weiss, S.A., Westlind, D.J., Woolley, T.J., Wright, M.C., 2022a. Fire and Tree Mortality Database (FTM), 2nd edition. Forest Service Research Data Archive, Fort Collins, CO. https://doi.org/10.2737/RDS-2020-0001-2.

Cansler, C.A., Kane, V.R., Hessburg, P.F., Kane, J.T., Jeronimo, S.M.A., Lutz, J.A., Povak, N.A., Churchill, D.J., Larson, A.J., 2022b. Previous wildfires and management treatments moderate subsequent fire severity. For. Ecol. Manag. 504, 119764. https://doi.org/10.1016/j.foreco.2021.119764.

Cansler, C.A., Wright, M.C., van Mantgem, P.J., Shearman, T.M., Varner, J.M., Hood, S. M., 2024. Drought before fire increases tree mortality after fire. Ecosphere 15, e70083. https://doi.org/10.1002/ecs2.70083.

Dinerstein, E., Olson, D., Joshi, A., Vynne, C., Burgess, N.D., Wikramanayake, E., Hahn, N., Palminteri, S., Hedao, P., Noss, R., Hansen, M., Locke, H., Ellis, E.C., Jones, B., Barber, C.V., Hayes, R., Kormos, C., Martin, V., Crist, E., Sechrest, W., Price, L., Baillie, J.E.M., Weeden, D., Suckling, K., Davis, C., Sizer, N., Moore, R., Thau, D., Birch, T., Potapov, P., Turubanova, S., Tyukavina, A., de Souza, N., Pintea, L., Brito, J.C., Llewellyn, O.A., Miller, A.G., Patzelt, A., Ghazanfar, S.A., Timberlake, J., Klöser, H., Shennan-Farpón, Y., Kindt, R., Lillesø, J.-P.B., van Breugel, P., Graudal, L., Voge, M., Al-Shammari, K.F., Saleem, M., 2017. An ecoregion-based approach to protecting half the terrestrial realm. BioScience 67, 534–545. doi:https://doi.org/10.1093/biosci/bix014.

Earth Resources Observation and Science (EROS) Center, 2020a. Landsat 5 Thematic Mapper Level-2, Collection 2 [dataset]. doi:10.5066/P9IAXOVV.

Earth Resources Observation and Science (EROS) Center, 2020b. Landsat 7 Enhanced Thematic Mapper Plus Level-2, Collection 2 [dataset]. U.S. Geological Survey. doi:10.5066/P9OGBGM6.

Earth Resources Observation and Science (EROS) Center, 2020c. Landsat 8–9 Operational Land Imager / Thermal Infrared Sensor Level-2, Collection 2 [dataset]. U.S. Geological Survey. doi:10.5066/P9OGBGM6.

Eidenshink, J., Schwind, B., Brewer, K., Zhu, Z.-L., Quayle, B., Howard, S., 2007. A project for monitoring trends in burn severity. Fire Ecol. 3, 3–21. https://doi.org/10.4996/fireecology.0301003.

Fernandez-Delgado, M., Cernadas, E., Barro, S., Amorim, D., 2014. Do we need hundreds of classifiers to solve real world classification problems? J. Mach. Learn. Res. 15, 3133–3181.

Furniss, T.J., Kane, V.R., Larson, A.J., Lutz, J.A., 2020. Detecting tree mortality with Landsat-derived spectral indices: improving ecological accuracy by examining uncertainty. Remote Sens. Environ. 237, 111497. https://doi.org/10.1016/j.rse.2019.111497.

Gorelick, N., Hancher, M., Dixon, M., Ilyushchenko, S., Thau, D., Moore, R., 2017. Google Earth Engine: planetary-scale geospatial analysis for everyone. Remote Sens. Environ. https://doi.org/10.1016/j.rse.2017.06.031.

Harvey, B.J., Andrus, R.A., Anderson, S.C., 2019. Incorporating biophysical gradients and uncertainty into burn severity maps in a temperate fire-prone forested region. Ecosphere 10, e02600. https://doi.org/10.1002/ecs2.2600.

Hudak, A.T., Fekety, P.A., Kane, V.R., Kennedy, R.E., Filippelli, S.K., Falkowski, M.J., Tinkham, W.T., Smith, A.M.S., Crookston, N.L., Domke, G.M., Corrao, M.V., Bright, B.C., Churchill, D.J., Gould, P.J., McGaughey, R.J., Kane, J.T., Dong, J., 2020. A carbon monitoring system for mapping regional, annual aboveground biomass across the northwestern USA. Environ. Res. Lett. 15. https://doi.org/10.1088/1748-9326/ab93f9.

Keeley, J.E., 2009. Fire intensity, fire severity and burn severity: a brief review and suggested usage. Int. J. Wildland Fire 18, 116–126.

Keeley, J.E., Safford, H.D., 2016. Fire as an ecosystem process. In: Mooney, H.A., Zavaleta, E. (Eds.), Ecosystems of California. University of California Press, Berkeley, CA, pp. 27–45.

Key, C.H., Benson, N.C., 2006. Landscape Assessment (LA). In: Lutes, D.C., Keane, R.E., Caratti, J.F., Key, C.H., Benson, N.C., Sutherland, S., Gangi, L. (Eds.), FIREMON: Fire Effects Monitoring and Inventory System RMRS-GTR-164-CD. USDA Forest Service, Rocky Mountain Research Station, Fort Collins, CO. https://doi.org/10.1002/app.1994.070541203.

Kolden, C.A., Smith, A.M.S., Abatzoglou, J.T., 2015. Limitations and utilisation of Monitoring Trends in Burn Severity products for assessing wildfire severity in the USA. Int. J. Wildland Fire 24, 1023–1028. https://doi.org/10.1071/WF15082.

Koontz, M.J., North, M.P., Werner, C.M., Fick, S.E., Latimer, A.M., 2020. Local forest structure variability increases resilience to wildfire in dry western U.S. coniferous forests. Ecol. Lett. https://doi.org/10.1111/ele.13447.

Lang, M., Binder, M., Richter, J., Schratz, P., Pfisterer, F., Coors, S., Au, Q., Casalicchio, G., Kotthoff, L., Bischl, B., 2019. mlr3: a modern object-oriented machine learning framework in R. J. Open Source Softw. 4, 1903. https://doi.org/10.21105/joss.01903.

Lutz, J.A., Struckman, S., Furniss, T.J., Cansler, C.A., Germain, S.J., Yocom, L.L., McAvoy, D.J., Kolden, C.A., Smith, A.M.S., Swanson, M.E., Larson, A.J., 2020. Large-diameter trees dominate snag and surface biomass following reintroduced fire. Ecol. Process. 9, 41. https://doi.org/10.1186/s13717-020-00243-8.

McCarley, T.R., Kolden, C.A., Vaillant, N.M., Hudak, A.T., Smith, A.M.S., Wing, B.M., Kellogg, B.S., Kreitler, J., 2017. Multi-temporal LiDAR and Landsat quantification of fire-induced changes to forest structure. Remote Sens. Environ. 191, 419–432. https://doi.org/10.1016/j.rse.2016.12.022.

McIver, J.D., Stephens, S.L., Agee, J.K., Barbour, J., Boerner, R.E.J., Edminster, C.B., Erickson, K.L., Farris, K.L., Fettig, C.J., Fiedler, C.E., Haase, S., Hart, S.C., Keeley, J. E., Knapp, E.E., Lehmkuhl, J.F., Moghaddas, J.J., Otrosina, W., Outcalt, K.W., Schwilk, D.W., Skinner, C.N., Waldrop, T.A., Weatherspoon, C.P., Yaussy, D.A., Youngblood, A., Zack, S., 2016. National Fire & Fire Surrogate Study Data: environmental effects of alternative fuel reduction treatments. Forest Service Research Data Archive, Fort Collins, CO: Forest. https://doi.org/10.2737/RDS-2016-0009.

Miller, J.D., Quayle, B., 2015. Calibration and validation of immediate post-fire satellite-derived data to three severity metrics. Fire Ecol. 11, 12–30. https://doi.org/10.4996/fireecology.1102012.

Miller, J.D., Safford, H.D., 2008. Sierra Nevada fire severity monitoring 1984–2004. Publication R5-TP-027. USDA-Forest Service, Pacific Southwest Region, Vallejo, CA, USA.

Miller, J.D., Thode, A.E., 2007. Quantifying burn severity in a heterogeneous landscape with a relative version of the delta Normalized Burn Ratio (dNBR). Remote Sens. Environ. 109, 66–80. https://doi.org/10.1016/j.rse.2006.12.006.

Miller, J.D., Knapp, E.E., Key, C.H., Skinner, C.N., Isbell, C.J., Creasy, R.M., Sherlock, J. W., 2009. Calibration and validation of the relative differenced Normalized Burn Ratio (RdNBR) to three measures of fire severity in the Sierra Nevada and Klamath Mountains, California, USA. Remote Sens. Environ. 113, 645–656. https://doi.org/10.1016/j.rse.2008.11.009.

Miller, J.D., Skinner, C.N., Safford, H.D., Knapp, E.E., Ramirez, C.M., 2012. Northwest California National Forests fire severity monitoring 1987–2008. Publication R5-TP-035. USDA-Forest Service, Pacific Southwest Region, Vallejo, CA, USA.

Miller, C.W., Harvey, B.J., Kane, V.R., Moskal, L.M., Alvarado, E., 2023. Different approaches make comparing studies of burn severity challenging: a review of methods used to link remotely sensed data with the Composite Burn Index. Int. J. Wildland Fire. https://doi.org/10.1071/WF22050.

Morgan, P., Keane, R.E., Dillon, G.K., Jain, T.B., Hudak, A.T., Karau, E.C., Sikkink, P.G., Holden, Z.A., Strand, E.K., 2014. Challenges of assessing fire and burn severity using field measures, remote sensing and modelling. Int. J. Wildland Fire 23, 1045–1060. https://doi.org/10.1071/WF13058.

Okoli, C., 2023. Statistical inference using machine learning and classical techniques based on accumulated local effects (ALE). arXiv 1–30. https://doi.org/10.48550/arXiv.2310.09877.

Okoli, C., 2025. Ale: interpretable machine learning and statistical inference with accumulated local effects (ALE). R package version 0.3.1. https://CRAN.R-project.org/package=ale.

Parks, S.A., Dillon, G.K., Miller, C., 2014. A new metric for quantifying burn severity: the Relativized Burn Ratio. Remote Sens. 6, 1827–1844. https://doi.org/10.3390/rs6031827.

Parks, S.A., Holsinger, L.M., Voss, M.A., Loehman, R.A., Robinson, N.P., 2018. Mean composite fire severity metrics computed with Google Earth Engine offer improved accuracy and expanded mapping potential. Remote Sens. 10, 879. https://doi.org/10.3390/rs10060879.

Parks, S.A., Holsinger, L.M., Koontz, M.J., Collins, L., Whitman, E., Parisien, M.-A., Loehman, R.A., Barnes, J.L., Bourdon, J.-F., Boucher, J., Boucher, Y., Caprio, A.C., Collingwood, A., Hall, R.J., Park, J., Saperstein, L.B., Smetanka, C., Smith, R.J., Soverel, N., 2019. Giving ecological meaning to satellite-derived fire severity metrics across North American forests. Remote Sens. 11, 1735. https://doi.org/10.3390/rs11141735.

Picotte, J.J., Arkle, R., Bastian, H., Benson, N., Cansler, A., Caprio, T., Dillon, G., Key, C., Klein, R.N., Kopper, K., Meddens, A.J.H., Ohlen, D., Parks, S.A., Peterson, D.W., Pilliod, D., Pritchard, S., Robertson, K., Sparks, A., Thode, A., 2019. Composite Burn Index (CBI) Data for the Conterminous US, Collected Between 1996 and 2018. https://doi.org/10.5066/P91BH1BZ.

Picotte, J.J., Bhattarai, K., Howard, D., Lecker, J., Epting, J., Quayle, B., Benson, N., Nelson, K., 2020. Changes to the Monitoring Trends in Burn Severity program mapping production procedures and data products. Fire Ecol. 16, 16. https://doi.org/10.1186/s42408-020-00076-y.

Powell, S.L., Cohen, W.B., Healey, S.P., Kennedy, R.E., Moisen, G.G., Pierce, K.B., Ohmann, J.L., 2010. Quantification of live aboveground forest biomass dynamics with Landsat time-series and field inventory data: a comparison of empirical modeling approaches. Remote Sens. Environ. 114, 1053–1068. https://doi.org/10.1016/j.rse.2009.12.018.

Probst, P., Boulesteix, A.-L., Bischl, B., 2019a. Tunability: importance of hyperparameters of machine learning algorithms. J. Mach. Learn. Res. 20, 1–32.

Probst, P., Wright, M.N., Boulesteix, A.-L., 2019b. Hyperparameters and tuning strategies for random forest. WIREs Data Min. Knowl. Discovery 9, e1301. https://doi.org/10.1002/widm.1301.

R Core Team, 2024. R: A Language and Environment for Statistical Computing. R Foundation for Statistical Computing, Vienna, Austria.

Radeloff, V.C., Roy, D.P., Wulder, M.A., Anderson, M., Cook, B., Crawford, C.J., Friedl, M., Gao, F., Gorelick, N., Hansen, M., Healey, S., Hostert, P., Hulley, G., Huntington, J.L., Johnson, D.M., Neigh, C., Lyapustin, A., Lymburner, L., Pahlevan, N., Pekel, J.-F., Scambos, T.A., Schaaf, C., Strobl, P., Woodcock, C.E., Zhang, H.K., Zhu, Z., 2024. Need and vision for global medium-resolution Landsat and Sentinel-2 data products. Remote Sens. Environ. 300, 113918. https://doi.org/10.1016/j.rse.2023.113918.

Reiner, A.L., Baker, C., Wahlberg, M., Rau, B.M., Birch, J.D., 2022. Region-specific remote-sensing models for predicting burn severity, basal area change, and canopy cover change following fire in the southwestern United States. Fire 5, 137. https://doi.org/10.3390/fire5050137.

Saberi, S.J., Harvey, B.J., 2023. What is the color when black is burned? Quantifying (re) burn severity using field and satellite remote sensing indices. Fire Ecol. 19, 24. https://doi.org/10.1186/s42408-023-00178-3.

Rodman, K.C., Andrus, R.A., Veblen, T.T., Hart, S.J., 2021. Disturbance detection in Landsat time series is influenced by tree mortality agent and severity, not by prior disturbance. Remote Sens. Environ. 254, 112244. https://doi.org/10.1016/j.rse.2020.112244.

Saberi, S.J., Agne, M.C., Harvey, B.J., 2022. Do you CBI what I see? The relationship between the Composite Burn Index and quantitative field measures of burn severity varies across gradients of forest structure. Int. J. Wildland Fire 31, 112–123. https://doi.org/10.1071/WF21062.

Steel, Z.L., Koontz, M.J., Safford, H.D., 2018. The changing landscape of wildfire: burn pattern trends and implications for California's yellow pine and mixed conifer forests. Landsc. Ecol. 33, 1159–1176. https://doi.org/10.1007/s10980-018-0665-5.

Stewart, J.A.E., van Mantgem, P.J., Young, D.J.N., Shive, K.L., Preisler, H.K., Das, A.J., Stephenson, N.L., Keeley, J.E., Safford, H.D., Wright, M.C., Welch, K.R., Thorne, J. H., 2021. Effects of postfire climate and seed availability on postfire conifer regeneration. Ecol. Appl. 31, e02280. https://doi.org/10.1002/eap.2280.

Strobl, C., Boulesteix, A.-L., Kneib, T., Augustin, T., Zeileis, A., 2008. Conditional variable importance for random forests. BMC Bioinf. 9, 307. https://doi.org/10.1186/1471-2105-9-307.

Theobald, D.M., Harrison-Atlas, D., Monahan, W.B., Albano, C.M., 2015. Ecologically-relevant maps of landforms and physiographic diversity for climate adaptation planning. PLoS One 10, e0143619. https://doi.org/10.1371/journal.pone.0143619.

Turner, M.G., 2010. Disturbance and landscape dynamics in a changing world. Ecology 91, 2833–2849. https://doi.org/10.1890/10-0097.1.

U.S. Geological Survey, 2025. 3D Elevation Program 10-Meter Resolution Digital Elevation Model.

van Mantgem, P.J., Nesmith, J.C.B., Keifer, M., Knapp, E.E., Flint, A., Flint, L., 2013. Climatic stress increases forest fire severity across the western United States. Ecol. Lett. 16, 1151–1156. https://doi.org/10.1111/ele.12151.

Viedma, O., Chico, F., Fernández, J.J., Madrigal, C., Safford, H.D., Moreno, J.M., 2020. Disentangling the role of prefire vegetation vs. burning conditions on fire severity in a large forest fire in SE Spain. Remote Sens. Environ. 247, 111891. https://doi.org/10.1016/j.rse.2020.111891.

Watson, D.S., Wright, M.N., 2021. Testing conditional independence in supervised learning algorithms. Mach. Learn. 110, 2107–2129. https://doi.org/10.1007/s10994-021-06030-6.

Welch, K.R., Safford, H.D., Young, T.P., 2016. Predicting conifer establishment post wildfire in mixed conifer forests of the North American Mediterranean-climate zone. Ecosphere 7. https://doi.org/10.1002/ecs2.1609.

Whitman, E., Parisien, M.-A., Thompson, D.K., Hall, R.J., Skakun, R.S., Flannigan, M.D., 2018. Variability and drivers of burn severity in the northwestern Canadian boreal forest. Ecosphere 9, e02128. https://doi.org/10.1002/ecs2.2128.

Williams, P.J., Kendall, W.L., Hooten, M.B., 2019. Selecting ecological models using multi-objective optimization. Ecol. Model. 404, 21–26. https://doi.org/10.1016/j.ecolmodel.2019.04.012.

Williams, J.N., Safford, H.D., Enstice, N., Steel, Z.L., Paulson, A.K., 2023. High-severity burned area and proportion exceed historic conditions in Sierra Nevada, California, and adjacent ranges. Ecosphere 14, e4397. https://doi.org/10.1002/ecs2.4397.

Wright, M.N., Ziegler, A., 2017. Ranger: a fast implementation of random forests for high dimensional data in C++ and R. J. Stat. Softw. 77, 1–17. https://doi.org/10.18637/jss.v077.i01.

Zhang, X., 2024. VIIRS/NPP Land Surface Phenology Yearly L3 Global 500m SIN Grid V002. https://doi.org/10.5067/VIIRS/VNP22Q2.002.